Polym. Korea, Vol. 46, No. 2, pp. 171-178 (2022)
https://doi.org/10.7317/pk.2022.46.2.171

ISSN 0379-153X(Print)
ISSN 2234-8077(Online)

뼈-인대 재생을 위한 경질 및 연질 구획을 갖는 생분해성 폴리우레탄 지지체

최강호*,**,# · 류영현*,**,# · 송민주*,**,# · 한수경*,** · 임하나*** · 김현종*** · 최성욱*,**,†

*가톨릭대학교 바이오메디컬화학공학과, **가톨릭대학교 생명공학과, ***한국생산기술연구원 표면처리기술 연구그룹

(2021년 10월 20일 접수, 2021년 11월 23일 수정, 2021년 12월 6일 채택)

Biodegradable Polyurethane Scaffolds with Hard and Soft Compartments for Potential Bone-to-tendon Regeneration

Kangho Choi*,,#, Young-Hyun Ryu*,**,#, Minju Song*,**,#, Soo Kyung Han*,**, Hana Lim***, Hyun-Jong Kim***, and Sung-Wook Choi*,**,†**

**Biomedical and Chemical Engineering, The Catholic University of Korea, 43 Jibong-ro, Wonmi-gu, Bucheon-si, Gyeonggi-do 14662, Korea*
***Department of Biotechnology, The Catholic University of Korea, 43 Jibong-ro, Wonmi-gu, Bucheon-si, Gyeonggi-do 14662, Korea*
****Surface Technology Group, Korea Institute of Industrial Technology (KITECH), Incheon 21999, Korea*

(Received October 20, 2021; Revised November 23, 2021; Accepted December 6, 2021)

초록: 뼈-힘줄 재생을 위해 양 끝에 뻣뻣한 구획과 유연한 구획을 갖는 폴리카프로락톤 기반 폴리우레탄 스캐폴드를 제작하였다. 폴리카프로락톤디올과 디이소시아네이트의 비율이 다른 수분산 폴리우레탄을 합성하여 스캐폴드의 양 끝이 각 구획에 적합한 인장 특성을 갖도록 제어하였다. 두 개의 구획이 있는 3차원 인쇄 폴리우레탄/폴리카프로락톤 스캐폴드는 염화칼슘에 의해 이온 가교되었고 스캐폴드의 딱딱한 구획은 교체 침지 방법을 사용하여 수산화인회석으로 개질하였다. 시험관 내 테스트에서 스캐폴드의 딱딱한 구획에서 조골 세포(MC3T3-E1)의 더 높은 증식 속도와 알칼리인산분해효소(ALP) 활성을 가지는 것을 확인하였으며, 근세포(C2C12)는 모든 구획에서 잘 증식하였다. 제어된 다공성 구조와 기계적 특성을 가지도록 3차원 인쇄된 폴리우레탄/폴리카프로락톤 스캐폴드는 뼈-인대 및 뼈-연골 및 뼈-힘줄의 재생에 대해 광범위하게 응용할 수 있다.

Abstract: Poly(ε-caprolactone) (PCL)-based polyurethane (PU) scaffolds with hard and soft compartments at either end were fabricated by fused deposition modeling (FDM) technique for potential bone-to-tendon regeneration. Waterborne-PU (WBPU) dispersions with different ratios of diisocyanate and PCL diol were synthesized to control the tensile properties suitable for either compartment at the end of the WBPU/PCL scaffolds. The three-dimensionally (3D) printed WBPU/PCL scaffold with two compartments was ionically cross-linked by calcium chloride, while the hard compartment of the scaffolds was further decorated by hydroxyapatite (HAp) using an alternative soaking method. *In vitro* tests revealed the higher proliferation rate and alkaline phosphatase (ALP) activity of osteoblastic cells (MC3T3-E1) on the hard compartment of the scaffold. Meanwhile, myocytes (C2C12) proliferated well on the soft compartment. We believe that the 3D printed WBPU/PCL scaffolds with controlled porous structure and mechanical property have wide potential applications for bone-to-ligament and bone-to-cartilage, as well as bone-to-tendon.

Keywords: 3D printing, polyurethane, tendon regeneration, ionic cross-linking, alternative soaking.

Introduction

Scaffolds are three-dimensional (3D) constructs that can mimic structural and biological environments and facilitate cell attachments and proliferation for the formation of desired tissues or organs. The chemical and physical characteristics of a scaffold, such as surface charge, pore size and interconnectivity, and mechanical strength, are basic factors for the growth and infiltration of cells and tissues within the scaffold.[1-3] The biological functions of a scaffold are also incorporated to enhance its performance. Therefore, scaffolds were decorated by or composed of many biological molecules, namely natural

#These authors equally contributed to this work.
†To whom correspondence should be addressed.
choisw@catholic.ac.kr, ORCID 0000-0002-5075-8798

polymers (*e.g.*, chitosan, gelatin, and collagen), proteins (*e.g.*, vascular endothelial growth factor and platelet-derived growth factor), and inorganics (*e.g.*, hydroxyapatite (HAp) and calcium phosphate).[4,5] All of these features should be considered in a controlled and balanced manner for successful tissue engineering.

Among the many target tissues and organs, the regenerations of the tendon attaching bone to muscle are still a great challenge, due to their complexity and heterogeneity in terms of structure and composition.[6] The two ends of the scaffold for tendon regeneration are required to have different characteristics that are suitable for each bone and muscle. The compartment contacting bone should be strong and hard, whereas the compartment contacting muscle should be ductile and soft.[7] In addition, collagen content increases gradually toward the muscle, whereas mineral content increases toward the bone.[8] Taking those features into account, previous works on tendon (or ligament) regeneration have focused on the multiphasic scaffolds with similar heterogeneity in mechanical strength and mineral content. The materials typically used for tendon regeneration are natural and synthetic polymers. The major drawbacks of most natural polymers are their low mechanical properties.[9,10] It is also difficult to obtain flexible and tough properties from synthetic polymers, such as polylactic acid (PLA), polycaprolactone (PCL), and their compositions.[11] For scaffold fabrication, electrospinning is one of the most often used techniques to develop scaffold for tendon regeneration. The electrospun scaffolds are usually modified with alternative soaking (A.S.) of calcium chloride and disodium hydrogen phosphate to have gradient mineral contents.[12] However, despite their unique extracellular matrix-like structure, the limited permeability of cells or tissues into the electrospun scaffold is considered a major obstacle to success in tendon regeneration. Considering the minimum pore size (above 100 μm) for bone formation,[13] the pore size of the electrospun scaffold is too small to induce bone formation. In addition, the lowered diffusion of nutrients and wastes throughout the electrospun scaffold, especially when fully covered by proliferated cells, was also pointed out as a challenging issue.[14] Besides electrospinning, a variety of fabrication methods, such as gas foaming,[15] solvent casting,[16] particle/salt leaching,[17] freeze-drying,[18] and microphase separation,[19] have been extensively developed to prepare well-defined scaffolds. However, in these approaches, the size, shape, and interconnectivity of pores cannot be precisely controlled.[20]

To address these issues, we selected a waterborne PCL-based polyurethane (WBPU) as a scaffold material and a fused deposition molding (FDM) technique as a fabrication method. We used a PCL diol as the first polyol for biocompatibility and biodegradability, and dimethylol propionic acid (DMPA) as a second polyol to enhance the hydrophilicity of the resultant scaffold. The advantage of typical polyurethane (PU) in tissue engineering is that the mechanical properties of the PU scaffold can be easily tuned within a wide range by the type and ratio of diisocyanate to polyol (NCO/OH).[21-23] The WBPU dispersions with different NCO/OH values were synthesized to demonstrate the hard and soft properties suitable for bone and muscle compartments, respectively. The 3D printing technique was utilized to develop 3D scaffolds with highly porous structure both inside, and at the outer surface. In addition, the compartment of the scaffold for bone was mineralized using the A.S. method to enhance the mechanical properties and osteoconductivity. The WBPU/PCL scaffold with hard and soft compartments could offer great potential for the regeneration of tissues, such as tendon and ligament, and others.

Experimental

Materials. WBPUs were synthesized by using a difunctional poly(ε-caprolactone) diol (PCL diol) (M_n=2000 g/mol) as a soft segment, 1,4-butanediol (BD) as chain extender, dibutyltin dilaurate (DBTDL) as a catalyst, and dimethylol propionic acid (DMPA) selected as an internal emulsifier. Triethylamine (TEA) was employed to neutralize the ionic groups in the dispersion. The reagents described above were provided by Sigma-Aldrich. Isophorone diisocyanate (IPDI) and acetone were obtained from the Tokyo Chemical Industry Co. (Tokyo, Japan). Acetone was used to control the viscosity during the synthesis.

Synthesis of Waterborne Polyurethanes. The biodegradable WBPU elastomers were synthesized by a water-based process. Table 1 provides the synthesis recipe. The reaction was carried out in a 1000 mL four-necked flask equipped with a mechanical stirrer, nitrogen inlet, and condenser. The soft segment consisted of PCL diol (M_n=2000 g/mol, Sigma-Aldrich, St. Louis, USA). The hard segment consisted of IPDI and two chain extenders DMPA and BD. DMPA was used as the hydrophilic chain extender. The molar feed ratio of IPDI/PCL diol/DMPA/BD was varied. In the first step, IPDI, PCL diol, DMPA, and 0.1% (w/w) of DBTDL were mixed at 90 °C and left to react for 5 h. After pre-polymerization, the reactor was then cooled to 50 °C and stirred for 30 min while the viscosity

Table 1. Recipe of WBPU12, WBPU15, and WBPU20 Dispersions (Unit : g)

Name	WBPU12	WBPU15	WBPU20
IPDI	21.55	24.25	28.73
PCL diol	80.00	72.00	64.00
DMPA	5.37	4.83	4.29
BD	1.46	3.28	5.83

was adjusted by adding acetone. The required amount of BD was then added, and the mixture was stirred to react for 2 h. TEA (molar ratio of DMPA to TEA=1:1) was dripped into the reactor to neutralize the carboxyl groups of DMPA. After 30 min of neutralization, deionized water (DW) was added under vigorous stirring for 1 h. Finally, the residual acetone was removed at 50 °C for 12 h, and the WBPU dispersion (30 wt%) was obtained. The average pH value of the WBPU dispersion was pH=7.30±0.21, which indicates that carboxylic groups had been successfully neutralized.[24,25]

Characterization of Waterborne Polyurethanes. The particle size distribution and zeta-potentials were analyzed by dynamic light scattering (DLS, Malvern Instruments, Zetasizer Nano ZS) at 25 °C. WBPUs were diluted with deionized water to a concentration of 0.5% (w/w) before measurements. Three measurements were performed for each dispersion. Weight average molecular weight (M_w) and polydispersity index (PDI) of the synthesized WBPU were determined by gel permeation chromatography (Waters Co., USA) equipped with a GPC KF-804 column, an HPLC pump (Waters 501), and a refractometer detector (Waters 410). Polystyrene standards and universal calibration were adapted to reduce measuring error. Tetrahydrofuran (THF, Sigma, St. Louis, USA) was used as a mobile phase at 0.8 mL/min flow rate and 1.0×10^3 Pa pump pressure, at 35 °C. Samples were prepared by dissolving the WBPU films in THF at 1% (w/w).

The mechanical properties of the WBPU films were evaluated by a universal testing machine (UTM, MCT-1150, A&D, Tokyo, Japan), and analyzed by the MSAT-Lite program (Version 1.1.1, A&D Co. Ltd., Japan). The WBPU films were cast on a smooth Teflon mold and dried at 50 °C for 1 day. The films were cut into a dog-bone shape specimen (length×width ×thickness, 10 mm×5 mm×0.4 mm), and tested. Crosshead speed of 10 mm/min was used for the tensile test. The properties of Young's modulus, tensile strength, and elongation at break were measured. Four measurements were made for each sample.

To compare different mechanical properties between the WBPU12 and WBPU20 films, each film was cut in the dimensions (length×wide×thickness, 5 mm×5 mm×0.4 mm), and then superglued together. The spatially differentiated tensile properties were observed in the same condition as above.

Fabrication of WBPU/PCL Scaffolds by 3D Printing. The WBPU/PCL scaffolds were printed with WBPU polymers and PCL using a 3D printer (EzROBO-5 GX ST2520, Eugene Technology, Yongin, Korea). WBPU films and PCL (M_n=80000 g/mol) pellets were mixed in a mass ratio of 4:1, and then the WBPU/PCL mixture was dissolved in dichloromethane (DCM) at a concentration of 20% (w/w). Next, the solution was poured into a smooth Teflon mold and dried at 30 °C for 1 day to obtain a WBPU/PCL composite film. For printing, the WBPU/PCL composite film (10 g) was filled in the 3D printer barrel and melted at 120 °C. Then, the WBPU/PCL fiber was extruded onto the platform through a 23 G nozzle at a constant pressure of 500 kPa and 1 mm/s extrusion speed.

The WBPU/PCL scaffold was submerged in $CaCl_2$ (200 mM) aqueous solution for 1 h to perform an ionic cross-linking reaction. The HAp formation on the scaffold was achieved by the A.S. process. Each scaffold was alternately submerged in two aqueous solutions containing calcium ions and phosphate ions. In detail, the scaffold was first submerged in 10 mL $CaCl_2$ (200 mM) aqueous solution at room temperature (RT) for 1 h and washed with DW. After DW washing, the scaffold was immersed in 10 mL Na_2HPO_4 (120 mM) aqueous solution at RT for 1 h and washed again using DW. This A.S. method was repeated three times to form HAp on the scaffold surface.

The surface morphology and topographical analysis of WBPU/PCL scaffolds were performed by scanning electron microscopy/energy-dispersive X-ray spectrometry (SEM/EDX S-4800, Hitachi, Tokyo, Japan). The mechanical properties of the scaffolds were analyzed using the UTM.

Cell Culture Study. Both MC3T3-E1 cells and C2C12 cells were cultured in growth medium. The growth medium was High-glucose Dulbecco's modified Eagle's medium (DMEM; WelGENE, Daegu, Korea) containing 10% (v/v) fetal bovine serum (FBS, WelGENE) and 1% (v/v) penicillin-streptomycin (WelGENE). MC3T3-E1 cells and C2C12 cells were incubated in 5% CO_2 at 37 °C. The medium was changed every 2 days.

Before cell seeding, the WBPU/PCL scaffolds were sterilized with ultraviolet (UV) for 6 h (3 h on each side), washed with phosphate-buffered saline (PBS) three times, and immersed in growth medium for a day. Cell suspension (40 μL, 1×10^7 cells/mL) was dripped at the top center of each WBPU/PCL

scaffold, and the scaffolds were incubated in a 48-well cell culture plate for 4 h to induce cell adhesion. The growth medium (400 μL) was then added. As a result, each well was seeded with 4×10^5 cells on the scaffolds, and incubated for (1, 3, and 7) days in an incubator (37 °C, 5% CO_2). The growth medium was changed every day.

Cell proliferation was measured using the cell counting kit-8 (CCK-8) at (1, 3, and 7) days after cell seeding, according to the manufacturer's instruction. For measurement, the culture medium was replaced by 400 μL of CCK-8 solution and incubated for 2 h. Following incubation, 100 μL of sample extract from each well was transferred to a 96-well plate, and their absorbance at 450 nm was measured by a microplate reader (Spectramax Plus 384, Molecular Devices, Co. Ltd., Philadelphia, USA).

Alkaline phosphatase (ALP) assay was measured at (1, 3, and 7) days after cell seeding. The WBPU/PCL scaffold was washed three times with PBS, and then 200 μL of extraction solution was treated. The cell lysis sample (50 μL) and p-nitrophenyl phosphate (pNPP, Sigma-Aldrich) solution (50 μL, 12.5 mM) were added to each well of the new 96-well plate. The plate was incubated at 37 °C for 30 min, and 50 μL NaOH (0.5 M) was added to finish the reaction. Subsequently, the absorbance at 405 nm was measured using a microplate reader.

ALP activity was calculated by dividing the pNPP quantitation by protein quantification. To measure the total protein content, the 2 μL cell lysis sample, 80 μL of DW, and 20 μL BioRad protein assay solution were added to each well of the 96-well plate. The absorbance at 595 nm was measured by a microplate reader.

Statistical Analysis. All the data presented are expressed as mean±standard deviation. Significance between the groups was evaluated by one-way ANOVA test (n=3).

Results and Discussion

Figure 1(a) shows the aqueous WBPU dispersions (20 wt%) prepared with different NCO/OH ratios. All the WBPU dispersions have remained stable for 6 months without sedimentation and aggregation. The WBPU dispersion with a higher NCO/OH ratio had more turbidity. The WBPU dispersion with an NCO/OH ratio of 1.2 was almost transparent, which is due to the extremely small particle size. Particle size distribution is a key parameter to evaluate the WBPU dispersion's stability. In general, large particle sizes (>1 μm) result in unstable dispersions due to the precipitation of the

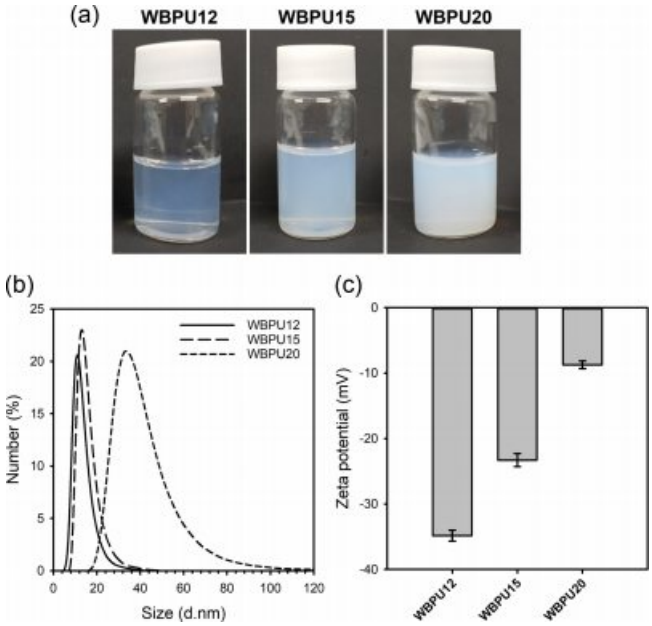

Figure 1. (a) Photographs; (b) average size; (c) zeta-potential of the WBPU dispersions prepared with different NCO/OH ratios.

largest particles. In contrast, smaller particles result in more stable dispersions, which allow storage for months. The particle size distribution of the WBPU dispersions was measured by DLS varying the NCO/OH molar ratios. Figures 1(b) and 1(c) show the average particle sizes and zeta-potential values of the three types of WBPU dispersions, respectively. Figure 1(b) shows that the lower NCO/OH ratio resulted in smaller particle size, which is due to the high content of the hard segment of diisocyanate. The WBPU 12 dispersion had an average size of 12.38±1.63 nm. The DMPA ratio to WBPU12, WBPU15, and WBPU20 were 4.96, 4.63, and 4.17%, respectively. Besides the content of the hard segment, the high ratio of hydrophilic DMPA in the WBPUs was attributed to the smaller particle size. In addition, Figure 1(c) shows that the high DMPA ratio resulted in a high zeta-potential value. The WBPU12 showed 34.85±0.83 mV, suggesting high colloidal stability. The M_w of WBPU dispersion varied from 33287 to 120898 g/mol with the increase in the NCO/OH molar ratio, which is due to the higher content of NCO groups.

To evaluate the tensile properties, WBPU films were prepared in a Teflon mold by drying at 50 °C. Figure 2(a) shows the representative stress-strain curves of the WBPU films. The increase in the NCO/OH ratio resulted in a more brittle property. This may be due to the increase in hydrogen bonding interactions between polyurethane chains with the higher ratio of the hard segment. Figures 2(b), 2(c), and 2(d) show Young's

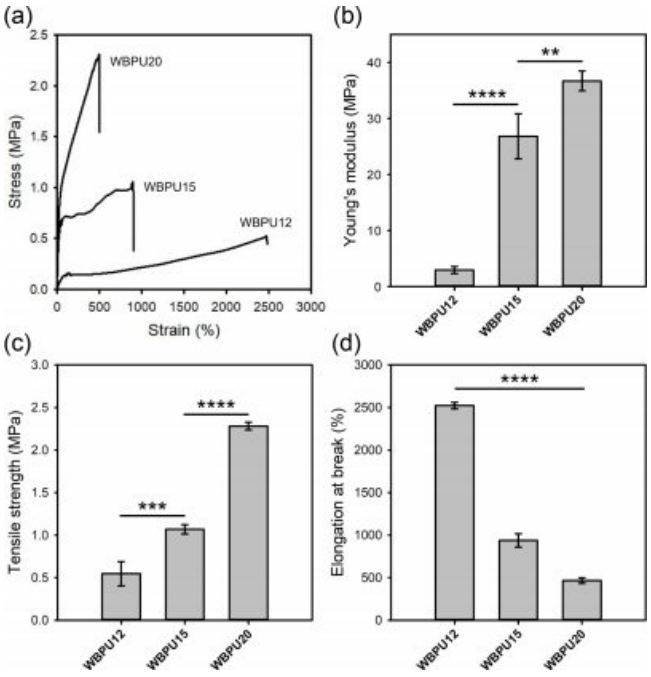

Figure 2. (a) Representative stress-strain curves; (b-d) tensile properties of the pristine WBPU films. *p<0.05, **p<0.01, ***p<0.001, ****p<0.0001 indicate significant differences between the two groups.

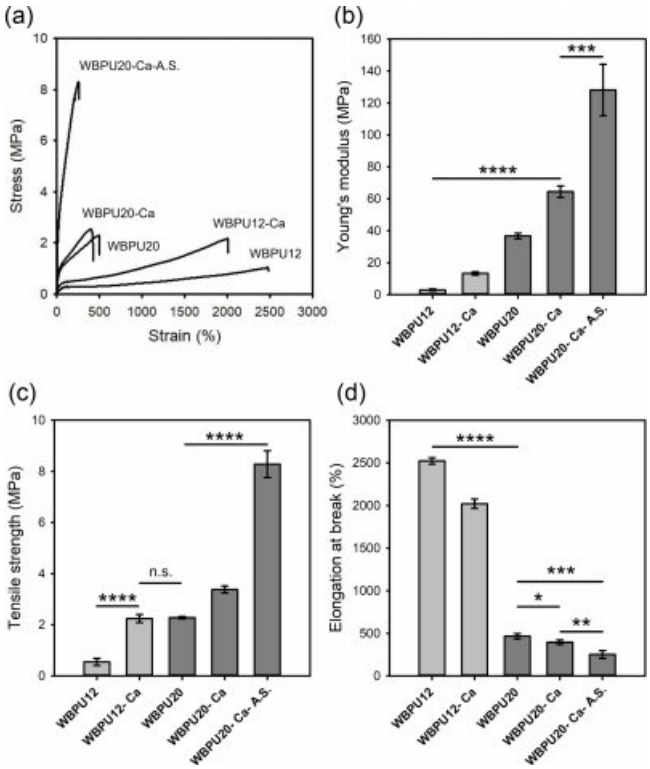

Figure 3. (a) Representative stress-strain curves; (b-d) tensile properties of the pristine, ionic-cross-linked, and A.S.-treated WBPU films. *p<0.05, **p<0.01, ***p<0.001, ****p<0.0001 indicate significant differences between the two groups.

modulus, tensile strength, and elongation at break of the WBPU films, respectively. The WBPU20 film had a higher Young's modulus of 36.7 MPa and tensile strength of 2.3 MPa. However, its elongation at break was 466.5%. The WBPU12 film showed an elongation at break of 2522.9%, suggesting a highly ductile property. These results confirmed that the tensile properties of the WBPU films were tuned by the NCO/OH ratio. Based on the results, WBPU20 and WBPU12 can be used as materials that are suitable for hard and soft tissue engineering, respectively.

The prepared WBPUs were originally water dispersible. Therefore, they should be cross-linked for implantable biomedical applications as a scaffold. Calcium chloride was chosen as an ionic cross-linker for the WBPUs with many carboxyl groups. In addition, the A.S. method was applied to further increase the tensile properties and decorate HAp on the surface. Figure 3 shows the tensile properties of the WBPU films before and after ionic cross-linking and the A.S. treatment. Figure 3(a) shows that the ionic cross-linking with calcium chloride increased Young's modulus and tensile strength, but decreased elongation at break. In addition, the A.S. treatment greatly improved the tensile properties of the WBPU20 film. The WBPU20 film after ionic cross-linking and A.S. treatment exhibited Young's modulus of 128.1 MPa, tensile strength of 8.3 MPa, and elongation at break of 251.4%. These results originate from the presence of HAp prepared by the A.S. method. Taken together, the ionic cross-linked WBPU12 can be suitable for soft tissue regeneration, while the ionic cross-linked and A.S.-treated WBPU20 can be suitable for hard tissue regeneration.

By considering the difference in tensile properties, the WBPUs can be applied to bone-to-tendon regeneration. Therefore, the WBPU film with soft and hard compartments was prepared using WBPU12 and WBPU20, respectively, and then ionically cross-linked. To demonstrate the difference in the ten-

Table 2. Sample Codes of WBPU-based Films or Scaffolds

Code	Polymer	Ca crosslinking	Alternative soaking
WBPU12	WBPU12	-	-
WBPU12-Ca	WBPU12	done	-
WBPU20	WBPU20	-	-
WBPU20-Ca	WBPU20	done	-
WBPU20-Ca-A.S.	WBPU20	done	done

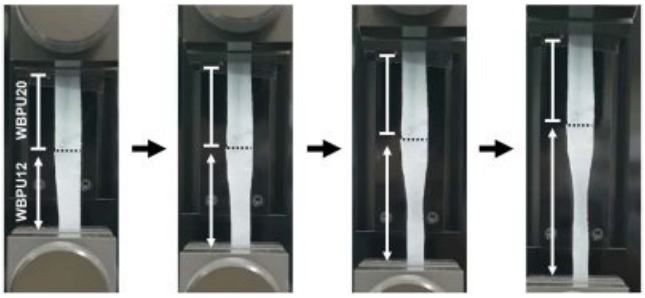

Figure 4. WBPU film composed of soft (WBPU12) and hard (WBPU20) compartments during elongation by UTM.

sile properties, the WBPU film with WBPU12 and WBPU20 compartments was elongated by UTM. Figure 4 shows that the lower compartment consisting of WBPU12 was elongated, whereas there was no change in length of the upper compartment consisting of WBPU20. Therefore, it can be confirmed that the WBPU12 and WBPU20 are favorable to tendon and bone tissue, respectively.

Figure 5(a) shows the SEM images of the pristine, ionic cross-linked, and ionic cross-linked and A.S.-treated WBPU20 scaffolds prepared by the 3D printing method. All the 3D printed scaffolds exhibited a well-defined structure. There was no significant difference in surface morphology between the pristine and ionic cross-linked scaffolds. However, rough morphology was observed at the surface of the ionic cross-linked and A.S.-treated WBPU20 scaffold. As shown in Figure 5(b), P and Ca were detected only on the A.S.-treated scaffold, confirming the presence of HAp on the surface. The HAp on the surface can facilitate the proliferation and differentiation of osteoblast.

To evaluate the effects of the tensile property and the presence of HAp on cell behavior, MC3T3-E1 and C2C12 cell lines were chosen as model cells for bone-to-tendon regeneration. Figure 6(a) shows that the ionic cross-linked WBPU20 scaffold had a slightly higher proliferation rate of MC3T3-E1 cells than did the ionic cross-linked WBPU12 scaffold. Furthermore, the ionic cross-linked and A.S.-treated WBPU20 scaffold exhibited the highest proliferation rate among the samples. For the C2C12 cells, there was no significant difference in the proliferation rate among the samples (Figure 6(b)). In all cases, C2C1C2 cells showed a higher proliferation rate than the MC3T3-E1 cells. Figure 6(c) shows the ALP activity of MC3T3-E1 cells cultured on the three types of scaffolds. The tendency of ALP activity was similar to the result of the proliferation rate, suggesting that the ionic cross-linked and A.S.-treated WBPU20 scaffold provided a suitable environment for MC3T3-E1 cell differentiation.

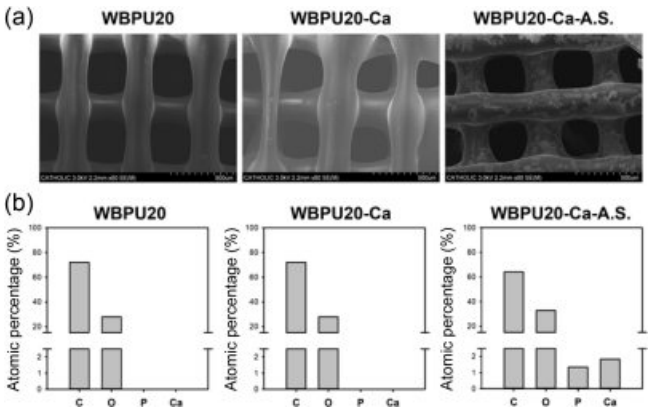

Figure 5. (a) SEM images; (b) elemental analysis of the pristine, ionic cross-linked, and A.S.-treated WBPU20 scaffolds.

Conclusions

We have demonstrated the fabrication of biodegradable WBPU/PCL scaffolds with hard and soft compartments at the

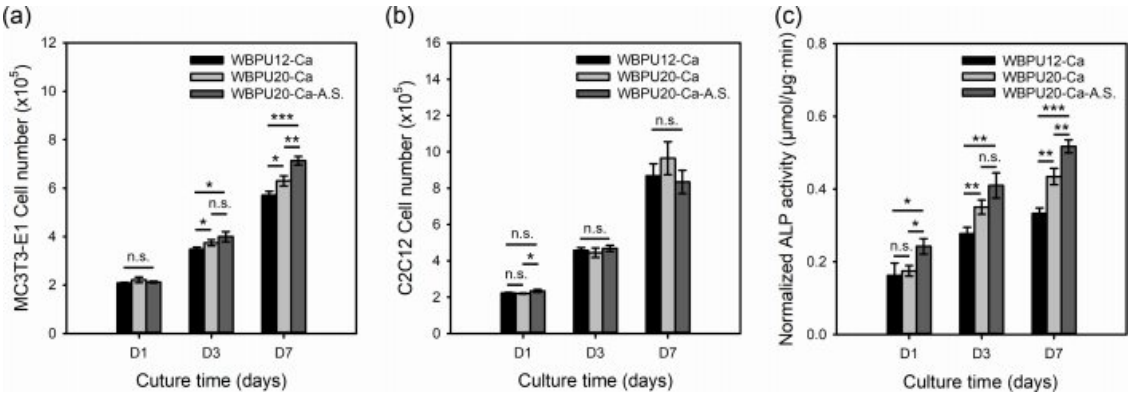

Figure 6. (a, b) Proliferation of MC3T3-E1 and C2C12 cells; (c) Normalized ALP activity of MC3T3-E1 cells cultured on the pristine, ionic cross-linked, and A.S.-treated WBPU scaffolds. *p<0.05, **p<0.01, ***p<0.001 indicate significant differences between the two groups.

ends using the FDM technique for potential tendon regeneration. The 3D printed WBPU/PCL scaffold was ionically cross-linked by calcium chloride, and the hard compartment contacting bone was further functionalized by HAp using the A.S. method. The two compartments of the scaffold provided the proper environment for the growth of bone and muscle tissue, respectively, in terms of mechanical properties and composition. At this stage, this work was focused on the synthesis and surface modification of WBPU-based scaffolds with different mechanical properties and the evaluation of their effect on the behaviors of osteoblasts and myocytes. We are planning to conduct more *in-vitro*/*in-vivo* experiments for the feasibility of bone-to-tendon regeneration. We believe that our approach has a wide range of applications, in particular for the interfaces between hard and soft tissues, such as tendon, ligament, and cartilage. In addition, the WBPU/PCL scaffolds can be further optimized to the desired tissue by combining other strategies, such as the composition of materials (*e.g.*, calcium phosphate, laponite, and collagen), loading of therapeutic agents (*e.g.*, bone morphogenetic protein, and kartogenin), and others.

Acknowledgment(s): This study was supported by the National Research Foundation of Korea (NRF) grant funded by the Korea government (MIST) (No. 2021R1A2C1003865), Korea Drug Development Fund funded by Ministry of Science and ICT, Ministry of Trade, Industry, and Energy, and Ministry of Health and Welfare (HN21C0317, Republic of Korea), and the Korea Medical Device Development Fund grant funded by the Korea government (the Ministry of Science and ICT, the Ministry of Trade, Industry and Energy, the Ministry of Health and Welfare, the Ministry of Food and Drug Safety) (202012D21-02).

Conflict of Interest: The authors declare that there is no conflict of interest.

References

1. Loh, Q. L.; Choong, C. Three-dimensional Scaffolds for Tissue Engineering Applications: Role of Porosity and Pore Size. *Tissue Eng. Part B Rev.* **2013**, 19, 485-502.
2. Ga, D.-H.; Lim, C.-M.; Jang, Y.; Son, T. I.; Han, D. K.; Joung, Y. K. Surface-modifying Effect of Zwitterionic Polyurethane Oligomers Complexed with Metal Ions on Blood Compatibility. *Tissue Eng. Regen. Med.* **2021**.
3. Choi, S. Y.; Li, M. X.; Kang, J. H.; Yang, D. H.; Joung, Y. K. Anti-thrombotic Polymer Surfaces Modified with Zwitterionic and Fluorinated Surface-migrating Oligomers. *Surf. Interfaces* **2021**, 25, 101280.
4. Casarrubios, L.; Gómez-Cerezo, N.; Sánchez-Salcedo, S.; Feito, M. J.; Serrano, M. C.; Saiz-Pardo, M.; Ortega, L.; de Pablo, D.; Díaz-Güemes, I.; Fernández-Tomé, B.; Enciso, S.; Sánchez-Margallo, F. M.; Portolés, M. T.; Arcos, D.; Vallet-Regí, M. Silicon Substituted Hydroxyapatite/VEGF Scaffolds Stimulate Bone Regeneration in Osteoporotic Sheep. *Acta Biomater.* **2020**, 101, 544-553.
5. Ghosh, M.; Halperin-Sternfeld, M.; Grigoriants, I.; Lee, J.; Nam, K. T.; Adler-Abramovich, L. Arginine-Presenting Peptide Hydrogels Decorated with Hydroxyapatite as Biomimetic Scaffolds for Bone Regeneration. *Biomacromolecules* **2017**, 18, 3541-3550.
6. Tits, A.; Ruffoni, D. Joining Soft Tissues to Bone: Insights from Modeling and Simulations. *Bone Rep.* **2021**, 14, 100742.
7. Lowen, J. M.; Leach, J. K. Functionally Graded Biomaterials for Use as Model Systems and Replacement Tissues. *Adv. Funct. Mater.* **2020**, 30, 1909089.
8. Spalazzi, J. P.; Boskey, A. L.; Pleshko, N.; Lu, H. H. Quantitative Mapping of Matrix Content and Distribution Across the Ligament-to-bone Insertion. *PLoS ONE* **2013**, 8, e74349-e74349.
9. Reddy, M. S.; Ponnamma, D.; Choudhary, R.; Sadasivuni, K. K. A Comparative Review of Natural and Synthetic Biopolymer Composite Scaffolds. *Polymers* **2021**, 13.
10. Abe, M. M.; Martins, J. R.; Sanvezzo, P. B.; Macedo, J. V.; Branciforti, M. C.; Halley, P.; Botaro, V. R.; Brienzo, M. Advantages and Disadvantages of Bioplastics Production from Starch and Lignocellulosic Components. *Polymers* **2021**, 13.
11. George, A.; Sanjay, M. R.; Srisuk, R.; Parameswaranpillai, J.; Siengchin, S. A Comprehensive Review on Chemical Properties and Applications of Biopolymers and Their Composites. *Int. J. Biol. Macromol.* **2020**, 154, 329-338.
12. Li, X.; Xie, J.; Lipner, J.; Yuan, X.; Thomopoulos, S.; Xia, Y. Nanofiber Scaffolds with Gradations in Mineral Content for Mimicking the Tendon-to-bone Insertion Site. *Nano Lett.* **2009**, 9, 2763-2768.
13. Venkatesan, J.; Vinodhini, P. A.; Sudha, P. N.; Kim, S.-K. Chapter Five - Chitin and Chitosan Composites for Bone Tissue Regeneration. *Adv. Food Nutr. Res.* **2014**, 73, 59-81.
14. Ameer, J. M.; Pr, A. K.; Kasoju, N. Strategies to Tune Electrospun Scaffold Porosity for Effective Cell Response in Tissue Engineering. *J. Funct. Biomater.* **2019**, 10, 30.
15. Mooney, D. J.; Baldwin, D. F.; Suh, N. P.; Vacanti, J. P.; Langer, R. Novel Approach to Fabricate Porous Sponges of Poly(*d,l*-lactic-*co*-glycolic acid) without the Use of Organic Solvents. *Biomaterials* **1996**, 17, 1417-1422.
16. Sin, D.; Miao, X.; Liu, G.; Wei, F.; Chadwick, G.; Yan, C.; Friis, T. Polyurethane (PU) Scaffolds Prepared by Solvent Casting/Particulate Leaching (SCPL) Combined with Centrifugation. *Mater. Sci. Eng.: C* **2010**, 30, 78-85.
17. Lee, S. B.; Kim, Y. H.; Chong, M. S.; Hong, S. H.; Lee, Y. M. Study of Gelatin-containing Artificial Skin V: Fabrication of Gelatin Scaffolds Using a Salt-leaching Method. *Biomaterials*

2005, 26, 1961-1968.
18. Wu, X.; Liu, Y.; Li, X.; Wen, P.; Zhang, Y.; Long, Y.; Wang, X.; Guo, Y.; Xing, F.; Gao, J. Preparation of Aligned Porous Gelatin Scaffolds by Unidirectional Freeze-drying Method. *Acta Biomater.* **2010**, 6, 1167-1177.
19. Ma, P. X.; Zhang, R. Microtubular Architecture of Biodegradable Polymer Scaffolds. *J. Biomed. Mater. Res.* **2001**, 56, 469-477.
20. Khorshidi, S.; Solouk, A.; Mirzadeh, H.; Mazinani, S.; Lagaron, J. M.; Sharifi, S.; Ramakrishna, S. A Review of Key Challenges of Electrospun Scaffolds for Tissue-engineering Applications. *J. Regen. Med. Tissue Eng.* **2016**, 10, 715-738.
21. Yan, R.; Jin, B.; Luo, Y.; Li, X. Optically Healable Polyurethanes with Tunable Mechanical Properties. *Polym. Chem.* **2019**, 10, 2247-2255.
22. Jang, J. Y.; Jhon, Y. K.; Cheong, I. W.; Kim, J. H. Effect of Process Variables on Molecular Weight and Mechanical Properties of Water-based Polyurethane Dispersion. *Colloids Surf. A: Physicochem. Eng. Asp.* **2002**, 196, 135-143.
23. Santamaria-Echart, A.; Arbelaiz, A.; Saralegi, A.; Fernández-d'Arlas, B.; Eceiza, A.; Corcuera, M. A. Relationship Between Reagents Molar Ratio and Dispersion Stability and Film Properties of Waterborne Polyurethanes. *Colloids Surf. A: Physicochem. Eng. Asp.* **2015**, 482, 554-561.
24. Athawale, V. D.; Kulkarni, M. A. Effect of Dicarboxylic Acids on the Performance Properties of Polyurethane Dispersions. *J. Appl. Polym. Sci.* **2010**, 117, 572-580.
25. García-Pacios, V.; Iwata, Y.; Colera, M.; Miguel Martín-Martínez, J. Influence of the Solids Content on the Properties of Waterborne Polyurethane Dispersions Obtained with Polycarbonate of Hexanediol. *Int. J. Adhes. Adhes.* **2011**, 31, 787-794.